Powder Technology 228 (2012) 349–358

Contents lists available at SciVerse ScienceDirect

Powder Technology

journal homepage: www.elsevier.com/locate/powtec

Characterization of the internal morphology of agglomerates produced in a spray fluidized bed by X-ray tomography

M. Dadkhah *, M. Peglow, E. Tsotsas

Thermal Process Engineering, Otto von Guericke University Magdeburg, Universitätsplatz 2, Magdeburg 39106, Germany

ARTICLE INFO

Article history:
Received 16 January 2012
Received in revised form 19 May 2012
Accepted 26 May 2012
Available online 31 May 2012

Keywords:
Spray fluidized bed agglomeration
X-ray micro-computer-tomography
Morphological descriptors

ABSTRACT

The internal structure of granules produced by spray fluidized bed agglomeration was investigated by means of X-ray micro-computer-tomography. The X-ray tomography delivers three-dimensional volume images, which are first used to count primary particles and derive center coordinate position, radius and volume for each of them. Further analysis by add-on algorithms results in a variety of morphological descriptors: radius of gyration, porosity, fractal dimension and pre-factor, coordination number distribution, and coordination angle distribution. Values and the behavior of these descriptors are presented and discussed for agglomerates consisting of a different number of primary particles, from 4 up to 310. The primary particles were made of porous γ-Al_2O_3, and they were nearly mono-dispersed and spherical. The distribution of solidified binder (hydroxyl-propyl-methylcellulose, originally as dilute solution in water) was not investigated. The agglomerates were produced in a top-spray fluidized bed at constant operating parameters.

1. Introduction

Fluidized bed agglomeration is a size enlargement process used to improve or modify the properties of small particles [1,2]. Typically, a solution of binder is sprayed on or in a bed of fluidized particles, so that the surface of the particles is wetted and liquid bridges are formed after interparticle collisions. The solvent – usually water – evaporates from the liquid into the fluidizing gas, forming solid bonds between the primary particles in the agglomerate [3,4]. Alternatively, a solidifying melt may be used [5]. Agglomerate properties depend on materials, the type of equipment used, and operating conditions [6,7]. Although spray fluidized bed agglomeration is widely applied in industry, the formulation of new products is still challenging. Wetting, drying and mixing occur simultaneously in the bed, therefore they are difficult to control independently. Final products have different microscopic structures, resulting in different macroscopic characteristics and end-use properties, such as strength, stability, flowability, rewetting, redispersion or active ingredient release [7,8].

Our understanding of spray fluidized bed agglomeration has been significantly enhanced by recently developed Monte Carlo simulation methods which implement many of the underlying micro-scale processes [3,4]. Such models can, for example, explain how the time necessary for the drying of deposited droplets influences the agglomeration rate. However, they are very coarse in respect to morphology, assuming spherical particles of a certain porosity, with a quite arbitrarily chosen value of $\varepsilon = 0.60$ [3,4].

The main reason for such coarse assumption is that the structure of agglomerates produced in spray fluidized beds has rarely been investigated in literature, despite its importance for both, process kinetics and end-user properties. The few existing publications concentrate on specific aspects, such as agglomerate shape (aspect ratio, circularity, roundness) [8], or porosity [9]. A similar lack of data exists for other wet agglomeration processes. In [10], porosities and pore size distributions are reported for agglomerates produced in high-shear or low-shear mixers, whereas the porosity of steam jet agglomerates was investigated in [11]. In [12], agglomerates were produced by dropping on a packed bed, consolidation in a rotary drum, and subsequent drying. However, analysis in this work aims at input data for discrete element simulation of agglomerate breakage, so that structural features are not really communicated.

The situation is better in respect to atmospheric aerosols [13] or agglomerates produced in flames [14–16], which may either be pollutants or nanoparticle products. Respective authors concentrate on the evaluation of fractal dimension and fractal pre-factor of the agglomerates. More parameters characterizing the morphology – so called morphological descriptors – can be derived for numerically simulated aggregates. Several authors have made use of this opportunity to different extents [17–23], though stressing the necessity of experimental validation of the purely computational results.

Concerning the experimental methods, the structure of flame-produced or atmospheric aggregates is usually investigated by means of light scattering or transmission electron microscopy (TEM) techniques [13,16]. Spray fluidized bed agglomerates consist of relatively large primary particles, so that light scattering is not applicable. The

* Corresponding author. Tel.: +49 391 67 18267; fax: +49 391 67 11160.
E-mail address: maryam.dadkhah@st.ovgu.de (M. Dadkhah).

0032-5910/$ – see front matter © 2012 Elsevier B.V. All rights reserved.
doi:10.1016/j.powtec.2012.05.051

TEM route appears to be attractive, but it provides only two-dimensional projected images, raising issues of transition to the real, three dimensional structure of the object [16]. Such issues are naturally removed in case of illumination from different angles and computational field reconstruction. Respective tomographic methods based on X-ray attenuation lead to genuine three dimensional information. They do not possess the resolution necessary in order to resolve the structure of nanoparticle aggregates, but they are very well applicable to granular and porous materials that consist of larger primary particles [24]. Despite its adequacy, the use of X-ray micro-computer-tomography (X-ray μ-CT) to investigate the structure of particles produced by wet agglomeration has until now been limited to very few studies, such as the previous reference [9] for spray fluidized bed agglomerates and the previous references [10,12] for agglomerates formulated by other wet processes. More results are available for consolidated materials, such as compacts produced from particles spray-dried at different conditions [25], see also the review in [24].

Due to the described lack of data, the present investigation seeks to contribute to a better understanding of the three-dimensional, internal morphology of spray fluidized bed agglomerates by means of X-ray μ-CT. First, materials and the experimental methods used for agglomerate production and structural analysis are presented. After a brief outline of image processing, the morphological descriptors considered are introduced and their evaluation is explained. Such descriptors are the radius of gyration, porosity, fractal dimension and pre-factor, coordination number distribution, and coordination angle distribution. Finally, respective results are presented and discussed. All the methods presented in this report are very effective for aggregates, the primary particles of which do not deviate too much from the spherical shape. It should be pointed out that the analysis concentrates on the spatial distribution of the primary particles. The spatial distribution of binder is, under certain conditions, also measurable, but outside of the scope of the present paper.

2. Materials and experimental methods

2.1. Agglomerate production

A total of 18 agglomerates consisting of 4 to 310 primary particles have been analyzed in the present work. The primary particles were made of porous γ-Al_2O_3 (Sasol GmbH, Germany) and they were nearly spherical and mono-dispersed. Measurements by Camsizer (Retsch Technologies GmbH, Haan, Germany) resulted in a very narrow range of primary particle diameters between 580 and 650 μm, an average diameter of 616 μm, and a high sphericity of 0.972.

Agglomeration was conducted in a batch-wise operated fluidized bed granulator with 300 mm inner diameter of the cylindrical fluidization chamber (customized construction by Pergande Co., Weißandt-Gölzau, Germany). The solution injected in top spray configuration consisted of water with 2% (mass fraction) hydroxyl-propyl-methyl-cellulose (HPMC, trade name Pharmacoat 606, from Shin-Etsus, Japan) as the binder. The nozzle provided by Düsen-Schlick GmbH, Untersiemau, Germany, model 940, was a two-fluid nozzle positioned 430 mm above the distributor plate, and 100 to 120 mm above the bed surface. By means of appropriate measuring and process control facilities all essential process parameters could be kept at constant values. These are air inlet temperature at 70 °C, fluidization air velocity at 1.7 m/s, and liquid spraying rate at 100 ml/min. The initial mass of bed material was 5 kg. Agglomerates consisting of different numbers of primary particles were extracted after different process times, up to 1 h.

2.2. X-ray tomography

The μ-CT equipment used in the present investigation was a customized device manufactured by ProCon X-ray GmbH, Garbsen, Germany, denoted by CT Procon alpha 2000. The X-ray source was operated at 45 kW and 350 μA. The agglomerate to be investigated was placed as close as possible to the tube and around 400 mm from the detector. By rotation of the sample holder, each agglomerate was scanned in the entire range of 0–360°. The increment of angle change was 0.45°, and three pictures were made at each projection angle, with an exposure time of 1.5 s. Typical acquisition time was about 1 h. The size of each voxel of the reconstructed volume is 5 μm. In this study each volume image consists of at least 600 two-dimensional images.

3. Image processing and image analysis

For image processing and quantitative analysis the MAVI software of the Fraunhofer Institute for Technical and Industrial Mathematics in Kaiserslautern, Germany, was used.

After scanning the samples in the μ-CT, we processed their volume images. This involved a sequence of operations to gain information from the image, as following:

(1) extraction of the region of interest
(2) binarization
(3) filtration, using reflective, double-edged filters
(4) segmentation, using pre-flooded watershed.

Fig. 1 shows images from the processing procedure. It should be noted that in Fig. 1b and c two-dimensional slices of the volume image are depicted. Fig. 2 shows, for two agglomerates, both the original image of the aggregate and the idealized Matlab drawing, based on data obtained from the processed image.

Using the data extracted from volume images, the primary particles contained in the agglomerate can be labeled and counted, providing the number of primary particles N_p per agglomerate. Center coordinates, radius and volume of each primary particle are identified and stored in matrices, which contain all the data needed for further evaluation.

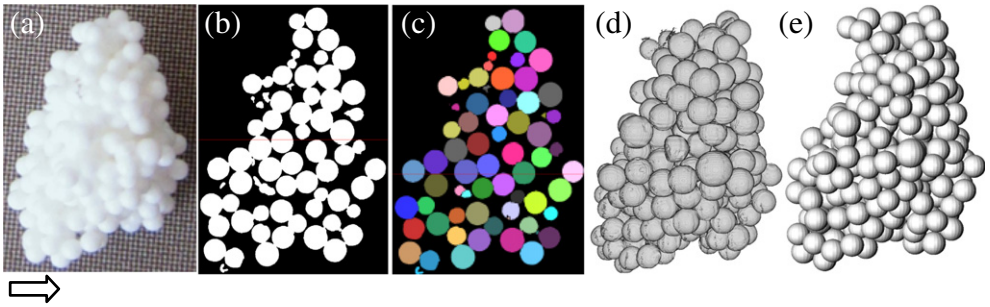

Fig. 1. Image processing procedure for primary particle identification and separation: (a) real agglomerate, (b) binarization, (c) segmentation, (d) μ-CT volume image, (e) idealized Matlab drawing.

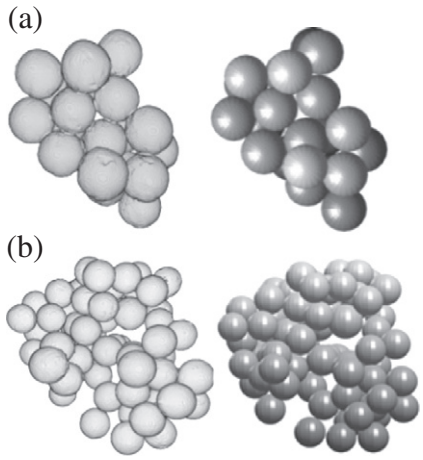

Fig. 2. Agglomerates containing (a) 21 primary particles, (b) 67 primary particles; in each case, the left-hand side picture is the original picture scanned in μ-CT, whereas the right-hand side picture shows the agglomerate structure redrawn in Matlab.

4. Morphological descriptors

Based on data gained from volume images, additional Matlab codes were developed to characterize particle morphology by means of the following morphological descriptors:

1. Radius of gyration
2. Porosity
3. Fractal dimension and pre-factor
4. Coordination number
5. Coordination angle

4.1. Radius of gyration

The radius of gyration, R_g, is one of the primary properties to characterize an aggregate. If the entire mass of an object were concentrated at the radius of gyration, then the moment of inertia would be the same as for the original object. Consequently, the radius of gyration describes the size of the object, but it also shows how the mass is distributed around the gravity center. The radius of gyration in respect to a point is defined as:

$$Rg = \sqrt{\frac{I}{M}} = \sqrt{\frac{1}{Np}\sum_{i=1}^{Np} Ri^2}. \quad (1)$$

Here, I is the moment of inertia, M is the mass of the aggregate

$$M = \sum_{i=1}^{Np} Mi. \quad (2)$$

M_i stands for the mass of the particle i, R_i is the distance of the primary particle from the considered point (usually the center of mass), and N_p is the number of primary particles in the aggregate.

For the purpose of computation, Eq. (1) can be transformed to

$$R_g = \sqrt{\frac{1}{2Np^2}\sum_{i=1}^{Np}\sum_{j=1}^{Np}\left(R_i - R_j\right)^2}, \quad (3)$$

see, for example, [21,26,27]. In Eq. (3), which has been used in the present work to evaluate the radius of gyration, R_i and R_j are the position vectors of the i'th and j'th primary particles from the center of mass. The result can be interpreted as a mean value for the radius of gyration, because Eq. (3) considers first the center of each primary particle as a reference point for the calculations, and then calculates the average of the resulting values over all primary particles. The main assumption is that all primary particles are of equal mass, which is closely fulfilled for the investigated agglomerates.

4.2. Porosity

Porosity – more precisely, the average volumetric porosity – of the agglomerates is defined as

$$\varepsilon = \left(1 - \sum_{i=1}^{Np} Vi/V\right), \quad (4)$$

where V_i is the volume of primary particle i, $\sum V_i$ is the sum of all primary particle volumes, and V is the total volume of the agglomerate. Primary particle volumes and their sum result directly from the μ-CT data. However, the total volume V is, obviously, a matter of definition. Three different approaches for evaluating porosity from the imaging results were examined in the present work and compared with each other, based on different derivations of the total volume.

4.2.1. Porosity from the radius of gyration

Assuming a spherical outer surface of the agglomerate with an equivalent radius, R_e, its central moment of inertia can be calculated to

$$I = \int_0^{Re} R^2 dM = \int_0^{Re} R^2.\rho.dV = \int_0^{Re} 4.R^4.\rho.\pi.dR = \frac{4.\pi.Re^5.\rho}{5}, \quad (5)$$

where ρ is the apparent density. At the same time, the volume of the agglomerate can be expressed by

$$V = \frac{4}{3}.\pi.Re^3, \quad (6)$$

and its mass by

$$M = \frac{4.\pi.Re^3.\rho}{3}. \quad (7)$$

Inserting Eqs. (5) and (7) in Eq. (1), the equivalent radius, R_e, is obtained as a function of the radius of gyration, R_g, to

$$Re = \sqrt{\frac{5}{3}}Rg. \quad (8)$$

With known radius of gyration, R_g, the equivalent radius, R_e, and then the total volume, V, Eq. (6), can be calculated. Inserting the latter in Eq. (4), agglomerate porosity is obtained.

Fig. 3 shows exemplarily the equivalent radius for one of the investigated agglomerates.

4.2.2. Porosity from convex hull

The convex hull of a set of points is by definition the smallest convex region containing all these points. The convex hull is typically represented by a sequence of the vertices of the line segments forming the polygonal boundary of an object, ordered along this boundary. In the present work the matrices of primary particle center coordinates and radii were used as the input data of a Matlab code that calculated and drawn the convex hull of each investigated agglomerate particle. Then, the volume within the convex hull was computed and set equal to the total volume of the agglomerate to calculate porosity by Eq. (4).

4.2.3. Porosity by dilation

Dilation is a basic operation in mathematical morphology. The main effect of the operator on an image is to gradually enlarge the boundaries of regions of foreground pixels. Thus areas of foreground pixels grow in size while holes within those regions become smaller. The mathematical

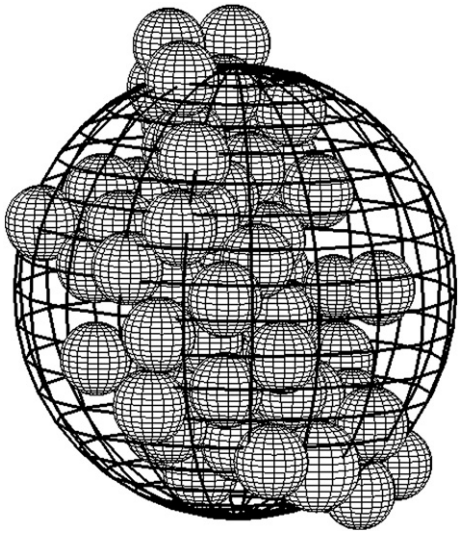

Fig. 3. Equivalent spherical boundary and equivalent radius for agglomerate containing 49 primary particles.

definition of dilation for grayscale images is, according to [28,29], as follows: suppose that X is the set of Euclidean coordinates corresponding to the input binary image, and that K is the set of coordinates for the structuring element. Let K_x denote the translation of K so that its origin is at x. Then the dilation of X by K is simply the set of all points x such that the intersection of K_x with X is non-empty.

Dilation takes two pieces of data as an input, an image to be dilated and a structuring element, which determines the precise details of the effect of the operator on the image and on the local pixel configuration. The structuring element consists of a pattern specified as the coordinates of a number of discrete points relative to some origin [30].

Grayscale dilation with an approximate ball as the structuring element was used in this study. Bright regions (the foreground) surrounded by dark regions (the background) grow in size, whereas dark regions surrounded by bright regions shrink in size. Small dark spots in images will disappear as they are filled by the surrounding intensity value. Small bright spots will become larger spots. The effect is most obvious at places in the image where the intensity changes rapidly. Regions of fairly uniform intensity will be largely unchanged, except at their edges.

Regarding the control of the dilation function, resolution and pixel size of the captured image were known via measurement in the present work, and the mean size of the primary particles was available from previous steps of the image data analysis. Therefore, the size of the structuring element could be defined in a way that helped to avoid that any unfilled volume remained within the volume image. The effect of dilation is illustrated in Fig. 4. Setting the volume of the dilated agglomerate equal to the total volume, V, Eq. (4) can again be applied to derive the porosity.

In Fig. 5 results of the three discussed procedures are schematically shown for an agglomerate with $N_p = 310$.

4.3. Fractal Dimension and Pre-factor

The fractal dimension, D_f, is a statistical quantity that gives an indication of how completely a fractal object can fill the space [31]. The value of D_f ranges from unity for strings to three for regular three-dimensional objects, and it can be a non-integer. Even if not strictly fractal, aggregates can be characterized by the fractal dimension [16], according to the statistical scaling law:

$$N_p = k_g \left(\frac{R_g}{r_i}\right)^{D_f}. \tag{9}$$

Here, R_g is the radius of gyration, r_i is the primary particle mean radius, and k_g is the fractal pre-factor (the so-called lacunarity [32]). Plotting the number of primary particles versus the ratio of the radii in logarithmic coordinates and linear regression immediately yield the fractal dimension from the slope and the pre-factor from the intercept.

4.4. Coordination number

The coordination number, CN, of a certain particle in a structure is the number of the contacts of this particle with surrounding particles. Apart from their morphological significance, mean coordination number and coordination number distribution (CND) can strongly affect aggregate properties, such as the mechanical strength or the effective thermal conductivity.

The coordination number is determined by calculation of the center–center distance between each primary particle and its associated neighbors. If this distance is equal or smaller than the sum of the radius of the primary particle and the radius of its considered neighbor, then one contact is counted to the CN. This evaluation is obviously sensitive to primary particle radius, r_i. Therefore, a different determination of r_i has been used in the present work for the derivation of CN and CA (see subsequent section) than for all other purposes. The usual determination throughout the work was by an equivalent sphere – i.e., perfect sphere containing the same amount of voxels as the primary particle – which is accurate enough at high sphericity (cf. Section 2.1). In the case of CN of CA, however, r_i was defined as the mean value of primary particle radii obtained in 13 discrete directions on the cuboidal lattice (three coordinate directions, six face diagonals and four space diagonals). Values of r_i obtained in this way were found to be systematically larger than the equivalent sphere values by about 3%. Their use in the determination of CN or CA guarantees that no contacts that should be counted are overseen.

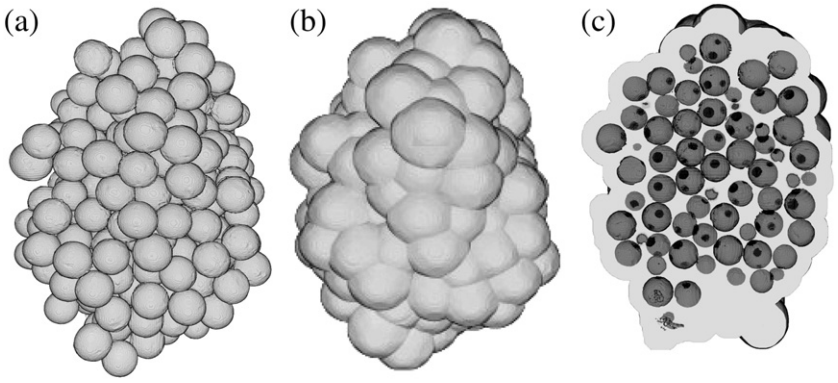

Fig. 4. (a) Volume image, (b) dilated picture, (c) subtraction of primary particles from the dilated image.

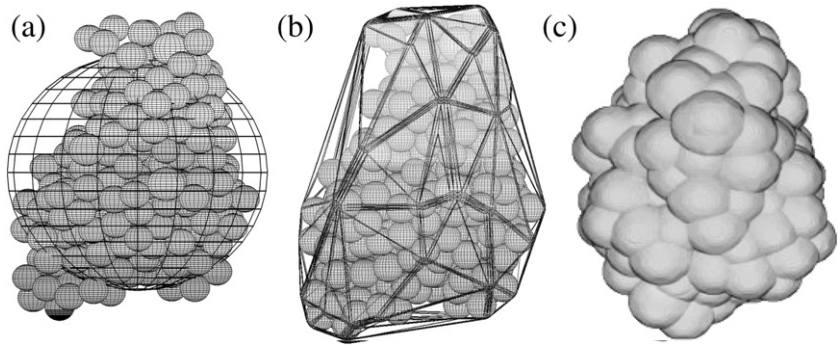

Fig. 5. Illustration of the three procedures to evaluate agglomerate porosity; (a) equivalent radius from gyration radius, (b) convex hull, (c) dilation.

4.5. Coordination angle

The coordination angle, θ, is defined as the angle between the vectors connecting the center of each primary particle to the centers of two of its contacting neighbors. If, for example, a particle has four contacting neighbors, then this particle also has four coordination angles, as illustrated in Fig. 6. In contrast to the scalar variables discussed until now, coordination angles and their distribution provide access to tensorial features of the considered aggregate. In the present work, all vectors connecting contacting primary particles were identified and the angles between them were evaluated by means of the dot product of vectors.

5. Results and discussion

Many of the results of the evaluation conducted on 18 agglomerates with different numbers of primary particles are summarized in Table 1. Notice that two of the agglomerate granules had, by coincidence, the same number of primary particles, namely $N_p = 71$. Those two granules are distinguished by a) and b).

A first finding concerns the average radius of primary particles in each agglomerate granule. The average of these averages is 317.6 μm, which means that the respective diameter of 635.2 μm corresponds within experimental and sampling accuracy to the Camsizer diameter of 616 μm from Section 2.1. Furthermore, the standard deviation of primary particle radii in Table 1 is, with about 5%, very small, in, again, good agreement to the Camsizer results.

Results concerning all evaluated morphological descriptors will be discussed in the following.

5.1. Radius of gyration

The values of gyration radius are difficult to immediately interpret, apart from the fact that R_g has – within a certain stochastic variation – the natural trend of increasing with increasing number of primary particles, N_p. However, an interpretation of R_g becomes possible by comparison with the maximum projected length (2D) of an aggregate, L, which has also been evaluated and is tabulated in Table 1. These results sum up to an average value of $L/(2R_g) = 1.715$ with a standard deviation of 8.7%.

Experimental data for flame-generated aggregates from [16], which include data from [14,15] and from some additional primary sources, show values of the ratio $L/(2R_g)$ located in the range 1.47 to 1.78. In [18], $L/(2R_g) = 1.50$ is reported for simulated aggregates of similar type. At a first glance, the present value of $L/(2R_g) = 1.715$ for spray fluidized bed agglomerates appears to be in the range of the literature values for flame generated aggregates. However, spray fluidized bed agglomerates are more compact in their structure than sooth and have a higher fractal dimension (cf. Section 5.3), so that one would expect for them $L/(2R_g)$-values at the lower end of the range of 1.47 to 1.78 for sooth, whereas the experimentally determined $L/(2R_g) = 1.715$ is at the upper end of the range. Application of theoretical equations that connect $L/(2R_g)$ with the fractal dimension from [16] leads with the fractal dimension $D_f = 2.611$ of the spray fluidized bed agglomerates (see Section 5.3) to $L/(2R_g)$-values from 1.33 to 1.36.

This is a certain contradiction, indicating that the fluffy, flame-produced aggregates from [16] – or the comparably fluffy simulated aggregates from [18] – differ from the spray fluidized bed aggregates not only in the fractal dimension, but also – to a certain extent – in the behavior of the ratio of maximal projected length to the radius of gyration and in the interrelation between fractal dimension and this ratio. Hence, $L/(2R_g)$ does not appear to be a good indicator of compactness or fluffiness when agglomerates produced in completely different ways are compared with each other. It should be noted that the present results cannot be compared with other data for spray fluidized bed agglomerates, or for other agglomerates of medium or high compactness, because such data cannot be found in literature.

5.2. Porosity

The results on average volumetric porosity obtained by the three different evaluation methods explained previously are listed in Table 1 and plotted in Fig. 7. The comparison shows that the three methods of evaluation are in relatively good agreement with each other. As to the influence of aggregate size, porosity appears to be low for small agglomerates and then increase to reach a plateau of rather constant values of about $\varepsilon = 0.63$. Very large agglomerate granules seem to have somewhat lower porosities, probably because such particles are old in respect to the time point of their extraction from the spray fluidized bed process, having experienced compaction by collisions with other particles and being the survivors of breakage events. Consequently, the plot of porosity shows a mild decrease at very large primary particle numbers.

It should be noted that the X-ray μ-CT used in the present work does not recognize the solidified binder, considering the respective volume as void. Therefore, the real porosity of the investigated agglomerates may have been somewhat lower than the porosity values of Table 1 and Fig. 7. However, such an effect is considered to be very small in our specific case, because very dilute binder solutions have been used (cf. with

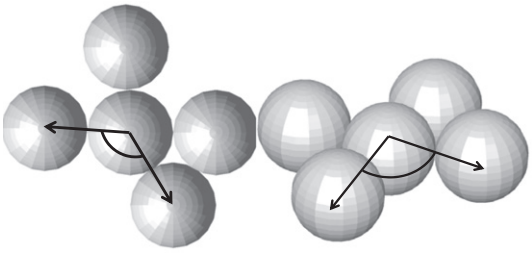

Fig. 6. Illustration of one coordination angle between a primary particle and its contacting neighbors.

Table 1
Result of evaluated porosity, coordination number and angles for all measured agglomerates.

N_p	r_i [μm]	R_g [μm]	L[μm]	$L/2R_g$	Porosity by R_g	Porosity by convex hull	Porosity by dilation	Mean CN	σ CN	Skewness CN	Frequent. Θ [degree]
4	323.2	513.3	1868.8	1.820	0.655	0.521	0.676	2	0.82	0	59
6	327.9	441.8	1598.9	1.809	0.430	0.255	0.525	4	0	–	56
17	329.1	835.1	2617.0	1.567	0.540	0.554	0.518	4.35	1.46	0.489	40
21	310.5	847.3	2945.0	1.738	0.540	0.501	0.562	4.38	1.47	0.191	61
36	311.8	1075.5	3585.5	1.667	0.652	0.617	0.547	3.22	1.42	0.701	61
40	311.5	1107.8	4001.9	1.806	0.614	0.580	0.580	3.85	1.44	0.213	60
49	325.4	1140.7	3815.7	1.672	0.558	0.564	0.546	4.16	1.65	0.439	60
67	319.7	1474.2	4751.5	1.612	0.746	0.693	0.725	3.97	1.76	0.484	60
71b	312.7	1544.4	5034.0	1.629	0.743	0.686	0.705	3.21	1.56	0.604	60
71a	314.5	1391.8	4587.0	1.648	0.557	0.551	0.582	4.90	1.68	0.247	59
88	313.2	1477.3	4877.6	1.651	0.630	0.613	0.622	4.36	1.82	0.462	60
121	316.3	1755.2	5977.8	1.703	0.689	0.631	0.628	3.57	1.32	0.299	60
146	312.4	1709.0	5759.8	1.685	0.630	0.681	0.624	3.94	1.83	0.542	60
170	321.7	1741.7	5891.9	1.692	0.595	0.627	0.629	4.35	1.75	0.173	60
186	314.8	2041.7	7184.3	1.759	0.705	0.696	0.637	3.65	1.59	0.351	60
270	316.1	2057.1	7562.0	1.838	0.601	0.595	0.515	5.53	1.81	−0.063	61
292	318.8	2083.2	7148.5	1.716	0.554	0.564	0.559	5.43	1.81	−0.141	59
310	318.3	2154.2	8084.2	1.876	0.576	0.578	0.575	5.48	1.80	−0.012	60

Section 2.1), the total mass of sprayed binder being much smaller than the mass of agglomerated primary particles. Additionally, the primary particles were porous, so that some of the binder penetrates them and solidifies in their interior (cf. with [4]). Such binder is utterly unimportant for the here considered external agglomerate porosity. As already indicated, binder distribution will be the topic of further research.

The mentioned value of $\varepsilon = 0.63$ is somewhat higher than the porosity values of about $\varepsilon = 0.58$ reported in [10] for agglomerates produced in mixers under conditions of low or moderate shear (denoted by LS and HS2 in the original paper). Conditions of really high shear (denoted by HS1) led to much more compact agglomerate granules with $\varepsilon = 0.124$ in the same work. Remarkably, the porosity assumed in [3,4] for the purpose of computation of the size of spray fluidized bed agglomerates simulated by means of Monte Carlo methods lies with $\varepsilon = 0.60$ quite exactly in between the value of about $\varepsilon = 0.63$ from the present work and $\varepsilon = 0.58$ from [10]. Taking scatter into account, the agreement between the present results and [3,4,10] can be considered as very good.

The same is true for the comparison with the porosity of simulated aggregates from [17]. In [17], porosity is analyzed in dependence of the freedom, or not, of primary particles to assume energetically more favorable positions by so called rolling events after their addition to the considered simulation box. Increasing number of allowed rolling events means restructuring and compaction of the resulting aggregates. In this way, aggregate porosity is obtained to $\varepsilon = 0.85$ without any rolling event, $\varepsilon = 0.62$ with one rolling event, $\varepsilon = 0.48$ with two rolling events, $\varepsilon = 0.44$ with three rolling events and, finally, $\varepsilon = 0.42$ at the limit of minimal potential energy for every primary particle considered.

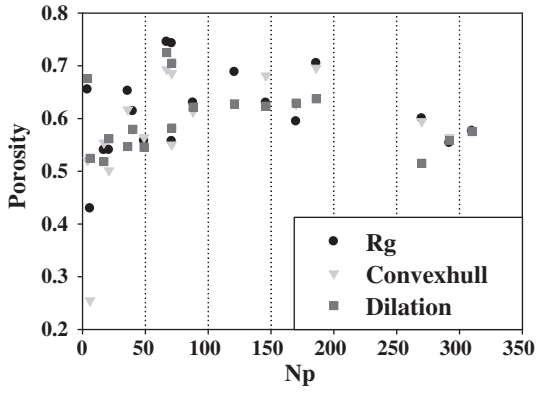

Fig. 7. Porosities evaluated by the three different methods versus number of primary particles per aggregate.

The present value of about $\varepsilon = 0.63$ agrees very well with the value of $\varepsilon = 0.62$ for one rolling event in [17], indicating moderate restructuring of fluidized bed agglomerates by particle–particle collisions and/or selective breakage. As already mentioned, large residence times in the fluidized particle system are in favor of restructuring and may, thus, lead to somewhat lower agglomerate porosity values. It should be noted that the potential influence of aggregate restructuring is also discussed in [19,20,33].

Surprisingly, much smaller measured porosities are reported in [9] for agglomerates produced in spray fluidized beds. These range between $\varepsilon = 0.20$ and $\varepsilon = 0.40$, increasing from the lower to the higher value with increasing mass fraction of the polymeric binder used. Such porosities are, as already indicated, rather typical of high shear than of fluidized bed granulation. The most likely explanation is that the water-soluble and soft materials used in [9] – namely mannitol, or a pharmaceutical excipient, or blends of them – led to compaction of the resulting agglomerates by sintering. Notice that the compacting influence of particle–particle overlap has been discussed in, among others, [20], based on simulation results.

The opposite behavior can be observed in the results from [11]. These show agglomerate porosities which start at more or less low values (down to $\varepsilon = 0.40$) to then increase with agglomerate size to very large porosities in the range of $\varepsilon = 0.70$ to 0.80. Apparently, the steam jet agglomeration process used in [11] produces fluffier granules than the spray fluidized bed process. The dependence of porosity on agglomerate size is assumed to be monotonically increasing with an asymptotic maximum in [11], which differs from the increasing-constant-decreasing trend of our present data. A more detailed discussion of this aspect is difficult, because information on the size of primary particles in the agglomerated food-component powders is missing from [11], so that the size of the resulting agglomerates cannot be reasonably scaled.

5.3. Fractal dimension and pre-factor

The double-logarithmic representation of Eq. (9) for our data is depicted in Fig. 8. As the figure shows, linearity is fulfilled with good accuracy. The values of fractal dimension and pre-factor obtained are $D_f = 2.611$ and $k_g = 1.617$, respectively. Linear regression without the first two points of the plot for the smallest agglomerates with $N_p = 4$ and 6 results with $D_f = 2.840$ in a somewhat higher value of the fractal dimension, and with $k_g = 1.121$ in a smaller value of the pre-factor.

For comparison, fractal dimensions in the range $D_f = 1.40$ to 1.86 are reported in [16] for aggregates produced in flames (see also [14,15], and the further primary literature from [16]). The respective pre-factors range from $k_g = 1.23$ to $k_g = 3.49$. The smaller fractal dimension of

flame aggregates in comparison to relatively compact spray fluidized bed agglomerates is an expected result. Scatter in the pre-factor is typically larger in literature, and its interpretation is more difficult.

The fractal properties of atmospheric aerosols are, according to [13], similar, but they have wider ranges of $D_f = 1$ to 2.5 and $k_g = 0.6$ to 8.0, with an average of about $k_g = 2.9$. However, a significant increase of D_f within the mentioned range with increasing number of primary particles is reported in [13]. This increase may be due to excessive restructuring by aging of the atmospheric aerosols, and it does not correspond to the behavior of spray fluidized bed agglomerates.

Finally, comparison is possible with an extended analysis of the fractal properties of simulated aggregates from [20]. There, aggregates have been composed either by particle–cluster (PC) or by cluster–cluster (CC) coalescence. In the PC-case, when every new aggregate is produced by addition of just one primary particle to an already existing aggregate, $D_f = 2.75$ and $k_g = 0.51$ was obtained. The very good agreement of fractal dimension with the present data indicates similarity in particle formation between spray fluidized beds and the PC-algorithm. Indeed, peculiarly shaped cluster–cluster aggregates are unlikely to survive collisions in a fluidized bed without either breaking or restructuring, which may give a selective advantage to particle–cluster combinations. Consequently, CC-aggregates from [20] with $D_f = 1.82$ and $k_g = 1.27$ rather resemble flame particles than spray fluidized bed granules. When accounting computationally for sintering in the CC-aggregates, the fractal dimension does not change, but the pre-factor increases up to $k_g = 2.21$. Simulated restructuring of CC-aggregates resulted in $D_f = 2.01$ and $k_g = 1.82$ [20], which is, again, much closer to the present results.

5.4. Coordination number

Average values of the coordination number are listed in Table 1 for every investigated agglomerate granule, and also plotted in Fig. 9. The distribution of coordination number is shown for four selected agglomerates with medium to large sizes in Fig. 10a, whereas Fig. 10b depicts the same information for the largest investigated granule ($N_p = 310$) in form of a histogram. Additionally, the standard deviation and the skewness of the CND are tabulated in Table 1.

The data for the two smallest agglomerates with $N_p = 4$ and $N_p = 6$ are not really significant in terms of coordination number, due to the very small number of primary particles involved. In case of $N_p = 4$ for example, one of the four primary particles had only one contact to other primary particles, two of them had two contacts each, and the fourth one had three contacts, resulting in an average CN equal to 2 and in zero skewness (perfectly symmetrical distribution) in Table 1. For the larger agglomerates, the mean coordination number appears to be rather constant at around CN = 4, whereas the three largest granules investigated show higher mean coordination numbers of about CN = 5.5 (Fig. 9). Concerning the CND, its standard deviation is rather constant throughout (Table 1). The skewness is also relatively constant, with the exception of the three largest agglomerates, which show a very low skewness of their CND, meaning that the CND becomes symmetrical and close to a normal distribution for these particles (Table 1, Fig. 10b). The described behavior means in Fig. 10a that the three agglomerates with $N_p = 40$, 88, 146 have most frequent CN-values in the vicinity of CN = 4. The lowest possible CN is unity, whereas the asymmetric CNDs tail above the most frequent CN towards the limit of the maximal possible CN, which is CN = 12 for nearly mono-dispersed and spherical primary particles (densest hexagonal regular arrangement).

There is a lack of measured CN data in literature, so that the present results can only be compared with results for simulated aggregates from [17] and [20]. There is excellent agreement between the present mean value of about CN = 4 for medium size aggregates and the value of CN = 3.99 from [17], which was computed for the case of primary particles allowed to experience one rolling event after their addition to an aggregate. This is fully consistent with the already discussed agreement between the present work and [17] regarding

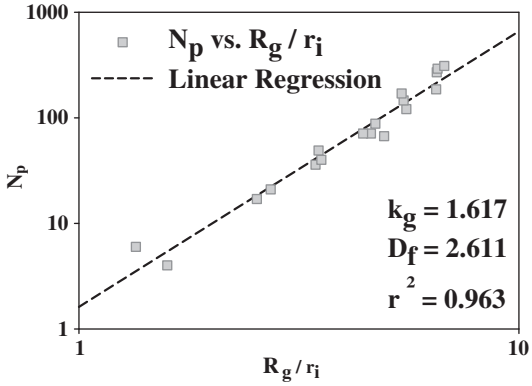

Fig. 8. Number of primary particles per aggregate vs. normalized radius of gyration.

aggregate porosity (Section 5.2). Our three biggest aggregates have larger mean coordination numbers, but they also have lower porosities, so that the consistency between coordination number and porosity still holds. These aggregates go into the direction of more than one rolling events in terms of the computational algorithm from [17], for which mean coordination numbers of around CN = 6 were predicted.

Concerning [20], their simulated particle–cluster aggregates have coordination number distributions that start at CN = 1 as the most frequent value and then decrease monotonically. Despite agreement in the fractal dimension (see Section 5.3), this behavior does not cope with measured CNDs from the present work (Fig. 10a). Cluster–cluster aggregates from [20] have a most frequent CN at two – which is too small in comparison to our data, and still too many primary particles with CN = 1. However, agreement with simulated CC-aggregates without restructuring could not be expected, because such aggregates are rather typical of flame-produced particles, as already discussed in Section 5.3. Increased coordination numbers are obtained in [20] after restructuring of the CC-aggregates, with most frequent values at CN = 3. Consequently, the restructuring operation appears to bring the simulated aggregates closer to the structure of spray fluidized bed agglomerates, as it was also the case for the fractal dimension. It should additionally be noted, that the dependence of the CND on the number of primary particles was always insignificant in [20]. This is in relatively good agreement with the present findings for medium size agglomerates (in exception of the three biggest ones).

5.5. Coordination angle

Coordination angle distributions are shown in Fig. 11a for several investigated agglomerates and in Fig. 11b for just one, with $N_p = 270$. The plots reveal that the sensitivity of CAD upon the number of primary

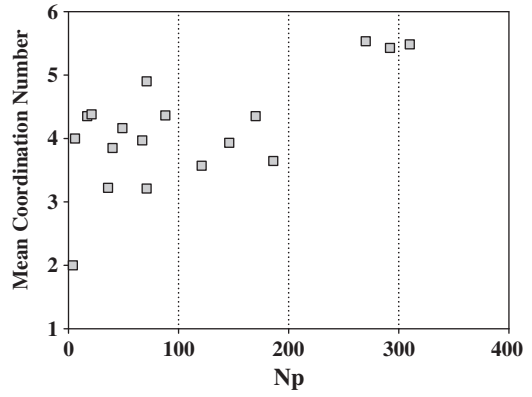

Fig. 9. Mean coordination number as a function of the number of primary particles.

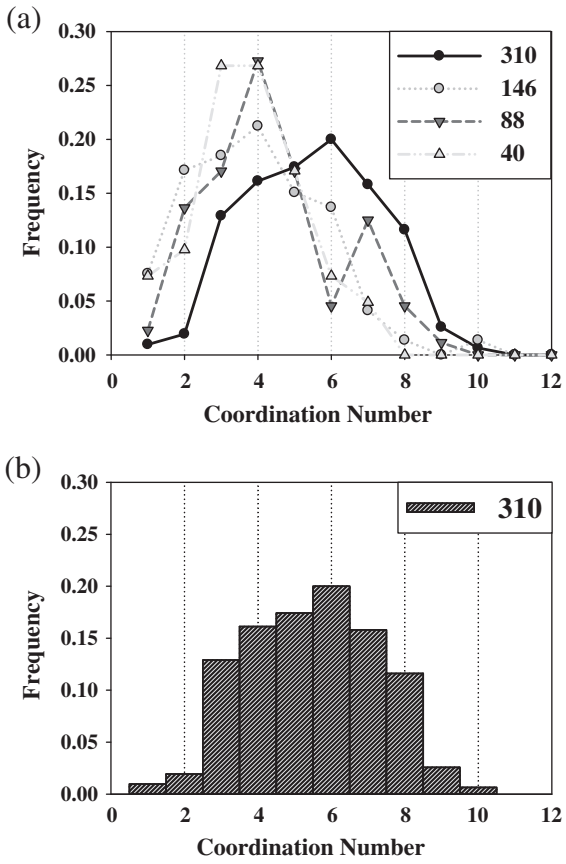

Fig. 10. (a) Coordination number distributions for four different agglomerates, (b) CND for the largest agglomerate granule in form of a histogram.

particles is low, and that the most frequent coordination angle is always at about 60°. Values of the most frequent CAs are also listed in Table 1, whereby CA is given as the integer center of 1° intervals. Non uniformities in the CAD, such as the secondary maximum in the histogram of Fig. 11b, may indicate some anisotropy in the structure.

Most frequent CAs at 60° and the shape of our measured CADs (Fig. 11) are in accordance with comparable simulation results from [20] for restructured CC-aggregates, cf. Sections 5.3 and 5.4. Additionally, the simulation results from [20] show the same independence of CAD from the number of primary particles as our present results. However, this similarity holds only for restructured CC-aggregates, whereas all other aggregates simulated in [20] – i.e. PC-aggregates, CC-aggregates without restructuring, sintered PC- or CC-aggregates – behave differently — their CADs are rather symmetrical and have much higher most frequent values. This is one more indication for the importance of agglomerate restructuring in fluidized beds.

6. Conclusions and outlook

The present work provided for the first time a comprehensive characterization of the internal structure of agglomerates produced in spray fluidized beds by means of X-ray micro-tomography. This characterization embraced the number of primary particles, maximal projection length, radius of gyration, porosity, coordination number distribution and coordination angle distribution for every investigated agglomerate granule, as well as their fractal properties (fractal dimension and pre-factor), with the following main conclusions:

- Concerning the porosity of produced agglomerates, spray fluidized beds are placed between flame, aerosol and steam jet agglomeration processes at the one side, and low shear mixers, sintering fluidized bed processes and high shear mixers at the other side – stated in a sequence of decreasing agglomerate porosity.
- The determined porosity values agree quite well with the porosity used in recent micro-process based Monte Carlo simulations of spray fluidized bed agglomeration [3,4]. In this way, the originally rather arbitrarily selected agglomerate porosity value of the simulations could be successfully verified.
- Furthermore, there is excellent agreement between the measured porosity values and the predictions of agglomerate formation algorithms with one rolling event after particle addition from literature [17].
- The present results on fractal dimension, coordination number and coordination angle compare with literature results for otherwise produced or simulated aggregates in a way which is consistent with the behavior of the porosity results.
- On contrary, the ratio of maximal projection length to the radius of gyration of the spray fluidized bed agglomerate granules is larger than expected from fractal dimension and flame aggregate results. Hence, this ratio does not appear to be a good indicator of compactness or fluffiness when comparing agglomerates produced in completely different ways.

In regard of the experimental method, X-ray micro-tomography was shown to be a powerful technique that can provide three-dimensional volume image data with the contrast and resolution necessary in order to derive detailed micro-structural information. Methods of digital image analysis which can be used to this purpose were presented and applied to real spray fluidized bed agglomerates.

It should be noted that most of the morphological descriptors derived from the X-ray μ-CT data are not accessible in any other way. As already

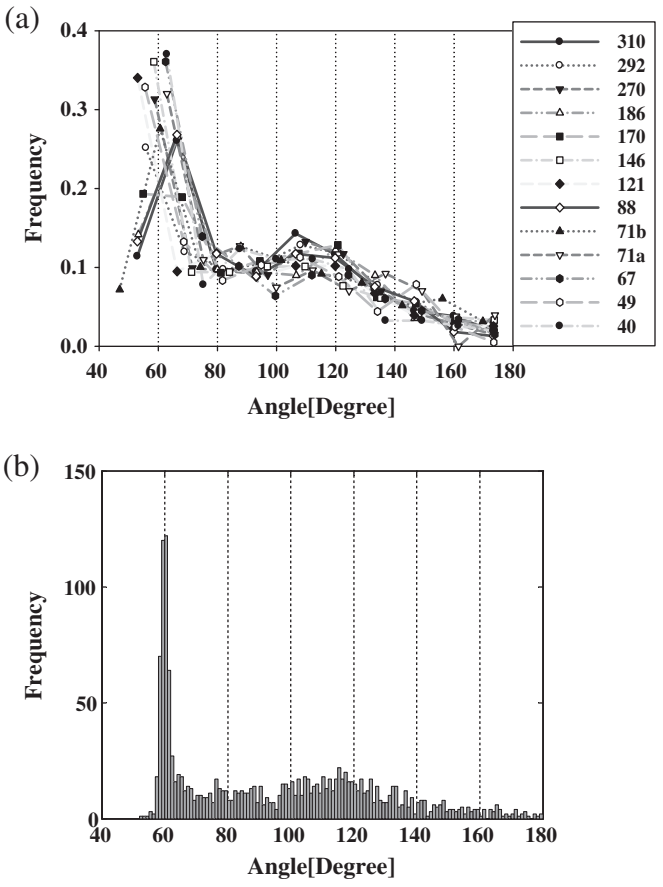

Fig. 11. (a) Coordination angle distributions for different agglomerates, (b) CAD for an agglomerate with $N_p = 270$ in form of a histogram.

pointed out in the introduction, light scattering is not applicable to aggregates consisting of relatively large primary particles, whereas TEM techniques are limited due to their two-dimensional nature. Standard methods that derive particle porosity from the comparison of apparent particle density to the skeletal density of the solid phase are accurate for nearly mono-dispersed and spherical particles. In any other case however, they either require severe, falsifying assumptions, or they must be upgraded by optical determination of the outer contour of single particles (see [11]), in a way that makes them comparably laborious to the X-ray μ-CT. Mercury porosimerty does not work properly with agglomerates, as previously pointed out in [11]. Such inherent deficiencies can explain the lack of data for even the porosity of spray fluidized bed agglomerates in the previous literature — with the exception of the already discussed values from [9], which were also obtained by means of X-ray μ-CT.

The most serious limitation that X-ray μ-CT has in common with other imaging techniques concerns the time and effort necessary for measurement and, especially, for data post-processing, which limits the number of objects that can be analyzed. Fortunately, the statistical significance of several investigated agglomerate properties increases with increasing number of primary particles in the compound. However, a larger number of investigated agglomerates – at best, a larger number of agglomerates with the same number of primary particles – would also be desirable. Continuing measurements will further contribute to this direction, though within a certain range of feasibility.

Apart from the quantitative augmentation of the set of data, work on mainly two further aspects is planned for the near future. First, the spatial distribution of solidified binder shall be investigated. Data of this kind do not exist in literature, but they would be valuable for, e.g., the further development of advanced Monte Carlo models of spray fluidized bed agglomeration (such as the model very recently presented in [34]). Second, essential parameters of the agglomeration process, which have been kept constant in the present work, shall be changed, and their influence on the resulting morphology shall be studied. The long term vision is to connect the morphology of particulate materials with, at the one side, process conditions and equipment involved in their production and, at the other side, their end-user properties. The presented morphological characterization is an essential step on this way.

Notation

D_f	fractal dimension
I	moment of inertia
k_g	pre-factor
L	maximum projected length of an aggregate
M	mass of an aggregate
M_i	mass of particle i
N_p	number of primary particles in an aggregate
r_i	mean radius of the primary particle
R_e	equivalent radius
R_g	radius of gyration
R_i	distance of primary particle from a considered point
V	total volume
V_i	volume of the primary particle
ε	porosity
θ	angle
ρ	density
σ	standard deviation

Abbreviations

μ-CT	micro-computer-tomography
CC	cluster–cluster
PC	particle–cluster
CN	coordination number
CND	coordination number distribution
CA	coordination angle
CAD	coordination angle distribution

Acknowledgments

The presented research took place in the frame of the graduate school “Micro-Macro-Interactions in Structured Media and Particle Systems” (GK 1554), funded by the Deutsche Forschungsgemeinschaft (DFG). The X-ray μ-CT device has been financed by the EFRD, European Fund for Regional Development (project no. 1211080002). The investigated agglomerates were produced by Dipl.-Ing. Torsten Hoffmann, in equipment funded by the German Ministry of Education and Research (BMBF, InnoProfile project NaWiTec).

References

[1] J. Litster, B. Ennis, The Science and Engineering of Granulation Processes, Kluwer Academic Publishers, Dordrecht, 2004.
[2] L. Mörl, S. Heinrich, M. Peglow, Fluidized bed spray granulation, in: A.D. Salman, M.J. Hounslow, J.P.K. Seville (Eds.), Handbook of Powder Technology, Vol. 11, Elsevier, 2007, pp. 21–188.
[3] K. Terrazas-Velarde, M. Peglow, E. Tsotsas, Investigation of the kinetics of fluidized bed spray agglomeration based on stochastic methods, AIChE Journal 57 (2011) 3012–3026.
[4] K. Terrazas-Velarde, M. Peglow, E. Tsotsas, Kinetics of fluidized bed spray agglomeration for compact and porous particles, Chemical Engineering Science 66 (2011) 1866–1878.
[5] H.S. Tan, A.D. Salman, M.J. Hounslow, Kinetics of fluidized bed melt granulation: the effect of process variables, Chemical Engineering Science 61 (2006) 1585–1601.
[6] S.H. Schaafsma, Down-Scaling of a Fluidised Bed Agglomeration Process, PhD-Thesis, University of Groningen, The Netherlands, 2000.
[7] M. Peglow, S. Antonyuk, M. Jacob, S. Palzer, S. Heinrich, E. Tsotsas, Particle formulation by spray fluidized beds, in: E. Tsotsas, A.S. Mujumdar (Eds.), Modern Drying Technology, Vol. 3, Wiley-VCH, Weinheim, 2011, pp. 295–378.
[8] C. Turchiuli, Z. Eloualia, N. Mansouri, E. Dumoulin, Fluidised bed agglomeration: agglomerates shape and end-use properties, Powder Technology 157 (2005) 168–175.
[9] P. Rajniak, C. Mancinelli, R.T. Chern, F. Stepanek, L. Farber, B.T. Hill, Experimental study of wet granulation in fluidized bed: Impact of the binder properties on the granule morphology, International Journal of Pharmaceutics 334 (1-2) (Apr 4 2007) 92–102.
[10] L. Farber, G. Tardos, J.N. Michaels, Use of X-ray tomography to study the porosity and morphology of granules, Powder Technology 132 (2003) 57–63.
[11] S. Hogekamp, M. Pohl, Porosity measurement of fragile agglomerates, Powder Technology 130 (2003) 385–392.
[12] D. Golchert, R. Moreno, M. Ghadiri, J. Litster, Effect of granule morphology on breakage behaviour during compression, Powder Technology 143 (2004) 84–96.
[13] C. Xiong, S.K. Friedlander, Morphological properties of atmospheric aerosol aggregates, Proceedings of the National Academy of Sciences of the United States of America 98 (21) (2001) 11851–11856.
[14] R.J. Samson, G.W. Mulholand, J.W. Gentry, Structural analysis of soot agglomerates, Langmuir 3 (2) (1987) 272–281.
[15] C.M. Megaridis, R.A. Dobbins, Morphological description of flame-generated materials, Combustion Science and Technology 71 (1990) 95–109.
[16] U.O. Koylu, Y. Xing, D.E. Rosner, Fractal morphology analysis of combustion-generated aggregates using angular light scattering and electron microscope images, Langmuir 11 (1995) 4848–4854.
[17] M. Tassopoulos, D.E. Rosner, Microstructural descriptors characterizing granular deposits, AIChE Journal 38 (1992) 15–25.
[18] A.M. Brasil, T.L. Farias, M.G. Carvalho, A recipe for image characterization of fractal-like aggregates, Journal of Aerosol Science 30 (10) (1999) 1379–1389.
[19] P. Tandon, D.E. Rosner, Monte Carlo simulation of particle aggregation and simultaneous restructuring, Journal of Colloid and Interface Science 213 (1999) 273–286.
[20] M. Brasil, T.L. Farias, M.G. Carvalho, U.O. Koylu, Numerical characterization of the morphology of aggregated particles, Journal of Aerosol Science 32 (2001) 489–508.
[21] M.A. Iati, A. Giusto, R. Saija, F. Borghese, P. Denti, Optical properties of composite interstellar grains: a morphological analysis, Astrophysical Journal 615 (2004) 286–299.
[22] M. Lagarrigue, J. Debayle, S. Jacquier, F. Gruy, J.C. Pinoli, Geometrical characterization of various shaped 3D-aggregates of primary spherical particles by radial distribution functions, Lecture Notes in Computer Science 6112 (2010) 434–443.
[23] M. Lapuerta, F.J. Martos, G. Martín-González, Geometrical determination of the lacunarity of agglomerates with integer fractal dimension, Journal of Colloid and Interface Science 346 (2010) 23–31.
[24] R. Moreno-Atanasio, R.A. Williams, X. Jia, Combining X-ray microtomography with computer simulation for analysis of granular and porous materials, Particuology 8 (2) (2010) 81–99.
[25] T.A. Deis, M. Lelovic, N.G. Eror, U. Balachandran, Effect of Ag doping on structure and critical temperature of $Bi_2Sr_2CaCu_2O_8+\delta$ superconductors, Applied Superconductivity 6 (6) (1998) 279–284.
[26] A.R. Khokhlov, Statistical Physics of Macromolecules, Amer Inst of Physics, 1994.

[27] P.J. Flory, Principles of Polymer Chemistry, Cornell Univ Pr, 1953.
[28] C.Gopal. Paul, C.R. Thomas, Characterisation of mycelial morphology using image analysis, Advances in Biochemical Engineering/Biotechnology 60 (1998) 1–59.
[29] R.C. Gonzalez, R.E. Woods, Digital Image Processing, third ed. Prentice Hall, Upper Saddle River, New Jersey, 2007.
[30] L. Wojnar, Image Analysis Application in Material Engineering, CRC Press, Boca Raton, 1999.
[31] R. Jullien, R. Botet, Aggregation and Fractal Aggregates, World Scientific Publ., Singapore, 1987.
[32] B. Mandelbrot, The Fractal Geometry of Nature, Freeman, New York, 1983.
[33] C. Artelt, H.J. Schmid, W. Peukert, On the relevance of accounting for the evolution of the fractal dimension in aerosol process simulations, Journal of Aerosol Science 34 (2003) 511–534.
[34] M. Dernedde, M. Peglow, E. Tsotsas, A novel, structure-tracking Monte Carlo algorithm for spray fluidized bed agglomeration, AIChE J. (2011), doi http://dx.doi.org/10.1002/aic.13709.